

# Numerical Heat Transfer, Part B: Fundamentals

## An International Journal of Computation and Methodology

ISSN: 1040-7790 (Print) 1521-0626 (Online) Journal homepage: [www.tandfonline.com/journals/unhb20](http://www.tandfonline.com/journals/unhb20)

## Optimum decomposition of the anisotropic diffusion term

F. Moukalled, L. Mangani & M. Darwish

To cite this article: F. Moukalled, L. Mangani & M. Darwish (2017) Optimum decomposition of the anisotropic diffusion term, Numerical Heat Transfer, Part B: Fundamentals, 72:3, 191-210, DOI: [10.1080/10407790.2017.1377534](https://doi.org/10.1080/10407790.2017.1377534)

To link to this article: <https://doi.org/10.1080/10407790.2017.1377534>



Published online: 25 Sep 2017.



Submit your article to this journal [↗](#)



Article views: 145



View related articles [↗](#)



View Crossmark data [↗](#)



## Optimum decomposition of the anisotropic diffusion term

F. Moukalled<sup>a</sup>, L. Mangani<sup>b</sup>, and M. Darwish<sup>a</sup>

<sup>a</sup>Department of Mechanical Engineering, American University of Beirut, Beirut, Lebanon; <sup>b</sup>Hochschule Luzern, Technik und Architektur, Horw, Switzerland

### ABSTRACT

A new decomposition method for the discretization of anisotropic diffusion term is developed. The method is a generalization of the optimum decomposition practice adopted in discretizing the isotropic diffusion flux. The new approach is applied in conjunction with the well-known semi-implicit and recently developed modified implicit nonlinear diffusion schemes and used for discretizing the anisotropic diffusion term. The resulting discretization methods are used for solving several anisotropic diffusion problems to compare the performance of the new decomposition technique with the standard one. Results generated demonstrate the virtues of the new method, which leads to a reduction in the CPU times needed for convergence by percentages reaching a level as high as 70%.

### ARTICLE HISTORY

Received 10 May 2017

Accepted 23 August 2017

### Introduction

In the initial development stage of the cell-centered finite volume method (FVM) [1–7], less work was performed on the discretization of diffusion term as compared to the work performed on the discretization of convection term [8–21]. This overlooking was due partly to the simplicity by which it can be discretized on orthogonal grids that dominated then and partly to the success of the central difference scheme in producing second-order accurate results without any numerical difficulty. Further developments in the method allowed solving problems in complex geometries but necessitated discretizing the diffusion term on nonorthogonal grids [22–33].

The discretization of diffusion flux on a body-fitted coordinate system was reported by Demirdzic [34]. Its discretization on unstructured grid systems using arbitrary polyhedral elements was reported by Muzaferija [35] and subsequently refined by Demirdzic and Muzaferija [36] and Mathur and Murthy [37]. This has led to the development of three different equations for the discretization of diffusion term [34–37]. Jasak [38] rederived these equations by decomposing the surface vector at an element face into two components with one always in the direction of the line connecting the centroids of the elements sharing the face. Depending on the magnitude of this component, or the direction of the second component, three equations can be retrieved. A chronological review of developments in the discretization of diffusion term was recently reported by Demirdzic [39]. Darwish and Moukalled [40] generalized the standard approach to deal with anisotropic diffusion by combining the diffusion coefficient tensor with the surface vector resulting in a modified surface vector.

The abovementioned techniques, which are designated here by the semi-implicit (SI) approach, decompose the diffusive flux into two parts. The first part, which is aligned with the grid direction, is treated implicitly, while the second part, which represents the nonorthogonal or cross-diffusion contribution, is handled explicitly in a deferred correction manner [41]. This semi-implicit approach results in an accurate evaluation of the diffusion term but leads, on highly skewed grid systems, to an

## Nomenclature

$C$	main grid point at an element centroid	$\mathbf{n}$	unit vector in the direction of $\mathbf{S}$
$\mathbf{d}_{CF}$	vector joining the two points $C$ and $F$	$\mathbf{n}'$	unit vector in the direction of $\mathbf{S}'$
$d_{CF}$	magnitude of $\mathbf{d}_{CF}$	$\mathbf{t}$	unit vector in the direction of $\mathbf{T}$
$\mathbf{e}_{CF}$	unit vector in the direction of $\mathbf{d}_{CF}$	$\mathbf{T}$	vector equal to $\mathbf{S} - \mathbf{E}$
$\mathbf{E}$	distance vector in the direction of $\mathbf{d}_{CF}$	$\mathbf{T}'$	vector equal to $\mathbf{S}' - \mathbf{E}'$
$\mathbf{E}'$	distance vector in the direction of $\mathbf{d}_{CF}$	$V$	cell volume
$E$	magnitude of $\mathbf{E}$	<b>Greek symbols</b>	
$E'$	magnitude of $\mathbf{E}'$	$\phi$	general variable
$F$	neighbor of element $C$	$\delta_C, \delta_F$	averaging factors
$f$	face	$\delta_C^*, \delta_F^*$	averaging factors satisfying Eq. (11)
$\mathbf{K}$	diffusion coefficient tensor	$\theta$	rotation angle
$k_{xx}, k_{xy}$	diffusion coefficients	$\xi, \eta$	curvilinear coordinates
$N_C$	location used in the calculation of the nonorthogonal part of the diffusion flux	<b>Subscripts</b>	
$N_F$	location used in the calculation of the nonorthogonal part of the diffusion flux	$C$	refers to main grid point
$Q$	source term in conservation equation	$f$	refers to element face
$\mathbf{S}$	surface vector	$F$	refers to the $F$ grid point
$\mathbf{S}'$	modified surface vector	<b>Superscripts</b>	
$S$	magnitude of $\mathbf{S}$	$T$	refers to the transpose of a vector
$S'$	magnitude of $\mathbf{S}'$	—	refers to an interpolated value

increase in the number of iterations to convergence and in certain cases to oscillations or divergence of the solution process due to the explicit treatment of the cross-diffusion part.

Several implicit schemes for discretizing the diffusion term in the context of the FVM have been developed over the years. This includes the multipoint flux approximation schemes [42, 43], the nonlinear diffusion schemes initially proposed by LePotier [44] and further expanded and refined by Lipnikov et al. [45–47], and others [48–50].

In a recent article, Darwish et al. [51] reported on a fully implicit scheme for the discretization of isotropic and anisotropic diffusion terms denoted by the modified implicit nonlinear diffusion (MIND) scheme applicable to a special set of variables that are not allowed to change sign. This requirement is not very restrictive, since many variables such as absolute temperature and pressure, turbulence quantities, and mass and volume fractions of species satisfy this condition. The method is a modification of the two-flux nonlinear diffusion method of Lipnikov [47] in combination with the ideas from the semi-implicit scheme. Similar to the semi-implicit method, the MIND scheme splits the surface or modified surface vector into two components with the possibility of adopting the three different approaches used with the semi-implicit scheme. While for the semi-implicit scheme, studies have shown that the contravariant decomposition is the most efficient [38], for the MIND scheme, no such studies have been conducted yet. Moreover, for the semi-implicit scheme, conducted studies dealt with isotropic diffusion and the conclusion drawn is based on that. No studies have been reported on the optimum decomposition of the more general anisotropic diffusion flux.

It is the purpose of this article to perform this task for both the semi-implicit and MIND schemes and to present a new decomposition of the modified surface vector, which is the optimum decomposition for the anisotropic diffusion flux. The new approach reduces to the same contravariant surface vector decomposition for isotropic diffusion.

In what follows, the diffusion equation of interest in this work is first presented. Then, the semi-implicit and MIND discretization schemes are reviewed along with the different decomposition practices of the surface/modified surface vector paving the way for introducing the new decomposition practice. Finally, several test problems are solved to assess the performance of the semi-implicit and MIND schemes with the newly modified surface vector decomposition option in comparison with the currently adopted decomposition approach.

## Governing equation

The diffusion equation of interest in this study can be written using vector notation as:

$$\underbrace{\nabla \cdot (\mathbf{K} \nabla \phi)}_{\text{diffusion term}} + \underbrace{Q}_{\text{source term}} = 0 \quad (1)$$

where  $\phi$  is the dependent variable,  $\mathbf{K}$  is the diffusion coefficient tensor, and  $Q$  is the source term. The FVM [1–4] is adopted to solve Eq. (1) numerically. Following this approach, the domain is subdivided into several nonoverlapping elements. The source term is computed by assuming the value of the dependent variable at the element centroid to represent the average value over the element volume. The discretization of the diffusion term is detailed next.

### Semi-implicit and modified implicit nonlinear diffusion schemes

A brief review of the semi-implicit [34–40] and MIND schemes [51] used for the discretization of diffusion term is given here. First the anisotropic diffusion term, with coefficient tensor  $\mathbf{K}$ , is reformulated in a form more suitable for the discretization process by switching the operation order as follows [40] (Figure 1(a)):

$$\begin{aligned} -\mathbf{K}_f \overline{\nabla \phi}_f \cdot \mathbf{S}_f &= -\overline{\nabla \phi}_f \cdot [\mathbf{K}_f]^T \mathbf{S}_f \\ &= -\overline{\nabla \phi}_f \cdot \mathbf{S}'_f \end{aligned} \quad (2)$$

where  $\mathbf{S}_f$  is the surface vector and  $\mathbf{S}'_f$  is the modified surface vector.

The derivations of the semi-implicit and MIND schemes start by decomposing the surface or the more general modified surface vector into two components such that

$$\mathbf{S}'_f = \mathbf{E}'_f + \mathbf{T}'_f \quad (3)$$

The various reported options for this decomposition [34–40] along with the newly suggested one will be detailed in the next section.

The discretization proceeds by linearizing the diffusion term along the component of  $\mathbf{S}'_f$  aligned with the CF direction, leading to

$$\overline{\nabla \phi}_f \cdot \mathbf{S}'_f = \frac{(\phi_F - \phi_C)}{d_{CF}} E'_f + \overline{\nabla \phi}_f \cdot \mathbf{T}'_f \quad (4)$$

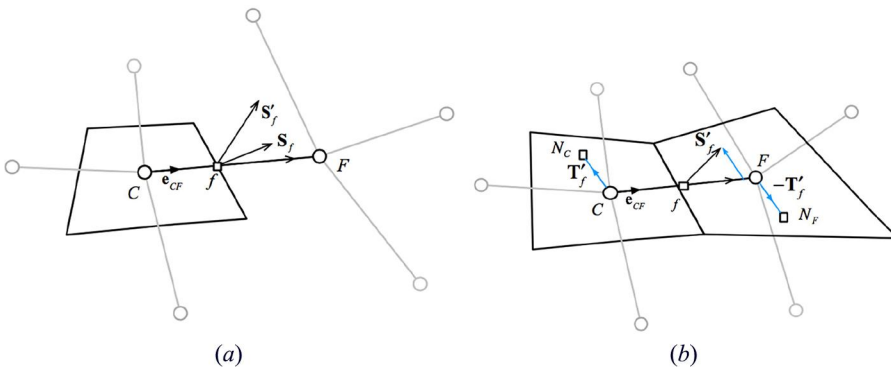


**Figure 1.** (a) The surface vector  $\mathbf{S}_f$  and the modified surface vector  $\mathbf{S}'_f$ ; (b) the modified nonlinear diffusion stencil.

In the semi-implicit scheme, the first term on the right-hand side of Eq. (4) is treated implicitly, while the underlined term is evaluated explicitly and added as a source in a deferred correction manner.

With the MIND scheme, instead of treating the underlined term in Eq. (4) explicitly, the average gradient appearing in that term is written as a linear combination of the gradients at the centroids of the elements sharing the face according to

$$\overline{\nabla\phi_f} = \delta_C \nabla\phi_C - \delta_F \nabla\phi_F \quad (5)$$

where  $\delta_C$  and  $\delta_F$  are weight factors that sum to 1. Using Eq. (5), the cross-diffusion term is transformed to

$$\overline{\nabla\phi_f} \cdot \mathbf{T}'_f = \delta_C \nabla\phi_C \cdot \mathbf{T}'_f - \delta_F \nabla\phi_F \cdot \mathbf{T}'_f \quad (6)$$

The terms in the above equation are evaluated as:

$$\begin{aligned} \nabla\phi_C \cdot \mathbf{T}'_f &= \frac{(\phi_{N_C} - \phi_C)}{d_{CN_C}} T'_f \\ \nabla\phi_F \cdot \mathbf{T}'_f &= \frac{(\phi_{N_F} - \phi_F)}{d_{FN_F}} T'_f \end{aligned} \quad (7)$$

where  $N_C$  and  $N_F$  are virtual nodes on opposite sides of the line joining  $C$  and  $F$  (Figure 1(b)) and the  $\phi_{N_C}$  and  $\phi_{N_F}$  values are computed using the gradients at  $C$  and  $F$ , respectively, as:

$$\begin{aligned} \phi_{N_C} &= \phi_C + \nabla\phi_C \cdot \mathbf{d}_{CN_C} \\ \phi_{N_F} &= \phi_F + \nabla\phi_F \cdot \mathbf{d}_{FN_F} \end{aligned} \quad (8)$$

The vectors  $\mathbf{d}_{CN_C}$  and  $\mathbf{d}_{FN_F}$  are of opposite directions and parallel to  $\mathbf{T}'_f$ , with their magnitudes related to length scales of the elements [51]. Combining Eqs. (4), (6), and (8), the discretized diffusion flux becomes

$$\overline{\nabla\phi_f} \cdot \mathbf{S}'_f = \left( \frac{E'_f}{d_{CF}} + \delta_F \frac{T'_f}{d_{FN_F}} \right) \phi_F - \left( \frac{E'_f}{d_{CF}} + \delta_C \frac{T'_f}{d_{CN_C}} \right) \phi_C + \delta_C \frac{T'_f}{d_{CN_C}} \phi_{N_C} - \delta_F \frac{T'_f}{d_{FN_F}} \phi_{N_F} \quad (9)$$

Similar to the Lipnikov method [47], the weight factors are computed to obey the relations

$$\begin{aligned} \delta_C + \delta_F &= 1 \\ \delta_C \frac{T'_f}{d_{CN_C}} \phi_{N_C} - \delta_F \frac{T'_f}{d_{FN_F}} \phi_{N_F} &= 0 \end{aligned} \quad (10)$$

yielding

$$\begin{aligned} \delta_C^\bullet &= \frac{\phi_{N_F}}{d_{FN_F}} / \left( \frac{\phi_{N_C}}{d_{CN_C}} + \frac{\phi_{N_F}}{d_{FN_F}} \right) \\ \delta_F^\bullet &= \frac{\phi_{N_C}}{d_{CN_C}} / \left( \frac{\phi_{N_C}}{d_{CN_C}} + \frac{\phi_{N_F}}{d_{FN_F}} \right) \end{aligned} \quad (11)$$

Substituting Eq. (11) into Eq. (9), the final form of the diffusion flux is obtained as:

$$\overline{\nabla\phi_f} \cdot \mathbf{S}'_f = \left( \frac{E'_f}{d_{CF}} + \frac{\phi_{N_C} T'_f}{\phi_{N_C} d_{FN_F} + \phi_{N_F} d_{CN_C}} \right) \phi_F - \left( \frac{E'_f}{d_{CF}} + \frac{\phi_{N_F} T'_f}{\phi_{N_C} d_{FN_F} + \phi_{N_F} d_{CN_C}} \right) \phi_C \quad (12)$$

With this treatment, a fully implicit discretization of the diffusion term is obtained.

Finally, it should be mentioned that in order for the MIND scheme to satisfy the discrete maximum/minimum principle [52, 53], a limiter may be applied on the gradients used in the calculation of  $\phi_{N_C}$  and  $\phi_{N_F}$ .

### New decomposition method of the modified surface vector

Three practices have been adopted for decomposing the vector  $S'_f$  [38, 39]: (i) by selecting the  $T'_f$  component to be orthogonal to  $S'_f$  to maximize the  $E'_f$  component (Figure 2(a)), (ii) by selecting the  $T'_f$  component to be orthogonal to  $E'_f$  to minimize the  $T'_f$  component (Figure 2(b)), or (iii) by setting the magnitude of the  $E'_f$  component equal to that of the original modified surface vector (Figure 2(c)). Mathematically, the expressions for  $E'_f$  and  $T'_f$  for the three different practices (i)–(iii) are given by:

$$(E'_f, T'_f) = \begin{cases} (i) & E'_f = \frac{S'_f \cdot S'_f}{e_{CF} \cdot S'_f} e_{CF} & T'_f = S'_f \left( \mathbf{n}'_f - \frac{1}{e_{CF} \cdot \mathbf{n}'_f} e_{CF} \right) \\ (ii) & E'_f = (e_{CF} \cdot S'_f) e_{CF} & T'_f = S'_f [\mathbf{n}'_f - (e_{CF} \cdot \mathbf{n}'_f) e_{CF}] \\ (iii) & E'_f = S'_f e_{CF} & T'_f = S'_f (\mathbf{n}'_f - e_{CF}) \end{cases} \quad (13)$$

where  $\mathbf{n}'_f$  is a unit vector in the direction of  $S'_f$  and  $e_{CF}$  is a unit vector along CF.

Experimentations with these decomposition practices for solving isotropic diffusion problems confirmed that option (i) is the most efficient. On the other hand, testing these practices with anisotropic diffusion problems revealed that option (i) is not the most efficient. In fact, options (ii) and (iii) performed better in many of the problems solved with no clear superiority of one method over the

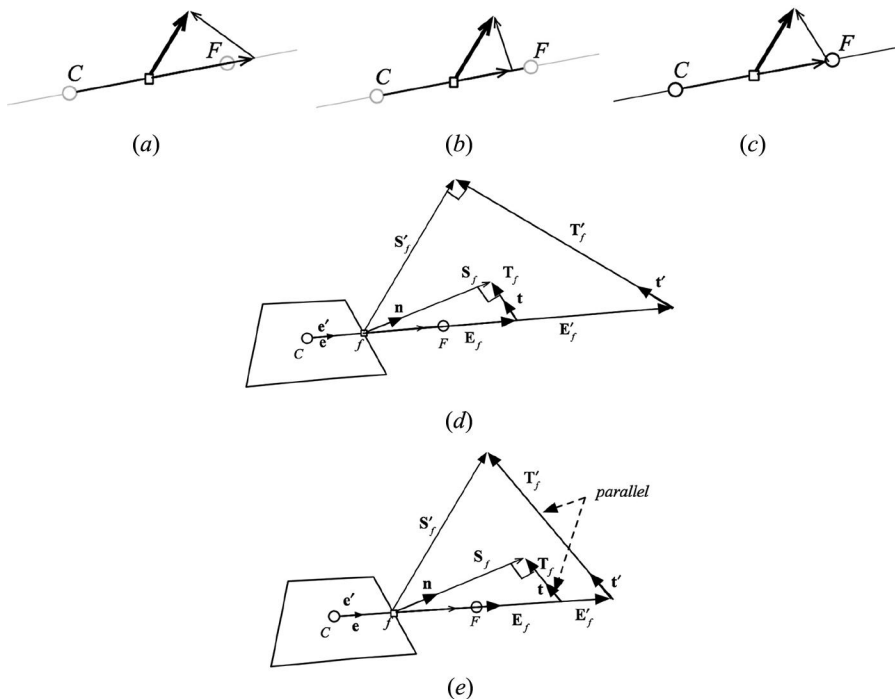


**Figure 2.** Decomposition of the surface/modified surface vector into two components by (a) maximizing the  $E_f/E'_f$  component, (b) minimizing the  $T_f/T'_f$ , and (c) setting the magnitude of the  $E_f/E'_f$  component equal to that of the original surface vector; (d) the standard decomposition of the modified surface vector (standard method); (e) the newly suggested decomposition of the modified surface vector in the directions of the contravariant components (contravariant method).

other but failed to converge in some of the test cases for no obvious reasons. This raised questions regarding the best decomposition practice for discretizing the anisotropic diffusion flux.

Referring back to the decomposition of the surface vector for the case of isotropic diffusion, the first approach is equivalent to decomposing the surface vector into its contravariant components and this approach is found to be more robust and more efficient than the other two decomposition techniques. As mentioned by Demirdzic [39], this is expected because it is the result of a direct discretization of the transport equations. Geometrically, this approach is equivalent to constructing the tangential component  $\mathbf{T}_f$  to be normal to the surface vector to maximize the  $\mathbf{E}_f$  component and thereby the implicit part of the diffusive flux. Since this tangential component is parallel to the face, the surface vector is actually decomposed into two components that are aligned with the grid system (the contravariant components). It is this property that should be satisfied in decomposing the modified surface vector, and not for the tangential component to be orthogonal to the modified surface vector (Figure 2(d)). Because the modified surface vector is not orthogonal to the face, the tangential component will be in a direction parallel to the face (Figure 2(e)). Therefore, the directions along which the modified surface vector should be decomposed are the same as the original surface vector (i.e., the contravariant components) with a unit vector in the  $\mathbf{E}_f$  or  $\mathbf{T}_f$  direction being also a unit vector in the  $\mathbf{E}'_f$  or  $\mathbf{T}'_f$  direction, respectively.

Denoting the unit vectors in the  $\mathbf{E}_f$  and  $\mathbf{T}_f$  directions by  $\mathbf{e}$  and  $\mathbf{t}$ , respectively, their values can be computed by decomposing the surface vector  $\mathbf{S}_f$  using the contravariant decomposition approach. Denoting by  $\mathbf{n}$  the outward unit vector normal to the face, and by  $\mathbf{d}_{CF}$  the distance vector connecting the  $C$  and  $F$  centroids, the expressions for  $\mathbf{e}$  and  $\mathbf{n}$  are given by:

$$\mathbf{e} = \frac{\mathbf{d}_{CF}}{d_{CF}} \quad \mathbf{n} = \frac{\mathbf{S}_f}{S_f} \quad (14)$$

Using  $\mathbf{e}$  and  $\mathbf{n}$ , the values of  $\mathbf{E}_f$  and  $\mathbf{T}_f$  following the contravariant decomposition approach, are found to be

$$\mathbf{E}_f = \frac{\mathbf{S}_f \cdot \mathbf{S}_f}{\mathbf{e} \cdot \mathbf{S}_f} \mathbf{e} \quad \mathbf{T}_f = S_f \left( \mathbf{n} - \frac{1}{\mathbf{e} \cdot \mathbf{n}} \mathbf{e} \right) \quad (15)$$

from which the unit vector  $\mathbf{t}$  is computed as:

$$\mathbf{t} = \frac{\mathbf{T}_f}{T_f} \quad (16)$$

Knowing the unit vectors in the  $\mathbf{E}'_f$  and  $\mathbf{T}'_f$  directions, Eq. (2) is rewritten as:

$$\begin{aligned} S'_x \mathbf{i} + S'_y \mathbf{j} &= E' \mathbf{e} + T' \mathbf{t} \\ &= E' (e_x \mathbf{i} + e_y \mathbf{j}) + T' (t_x \mathbf{i} + t_y \mathbf{j}) \\ &= (E' e_x + T' t_x) \mathbf{i} + (E' e_y + T' t_y) \mathbf{j} \end{aligned} \quad (17)$$

from which the  $\mathbf{E}'_f$  and  $\mathbf{T}'_f$  vectors are calculated as:

$$\left. \begin{aligned} S'_x &= E' e_x + T' t_x \\ S'_y &= E' e_y + T' t_y \end{aligned} \right\} \Rightarrow E' = \frac{S'_x t_y - S'_y t_x}{e_x t_y - e_y t_x} \Rightarrow \mathbf{E}' = \frac{S'_x t_y - S'_y t_x}{e_x t_y - e_y t_x} \mathbf{e} \Rightarrow \mathbf{T}' = \mathbf{S}' - \mathbf{E}' \quad (18)$$

## Results and discussion

The performance of the newly suggested method for decomposing the modified surface vector arising in the discretization of anisotropic diffusion term in the contravariant directions (Figure 2(e)) is

evaluated by comparison with the standard decomposition approach shown in Figure 2(d). The assessment is performed for both the MIND and the semi-implicit schemes by solving a set of anisotropic diffusion problems on grids with quadrilateral elements of different skewnesses and density. Results are reported in terms of CPU time and residual reduction plots. For all predictions, computations are continued until the maximum absolute residual in the domain drops below  $10^{-8}$ .

Since structured grid systems are used, the TDMA algorithm is used to solve the algebraic systems of equations for all problems presented in this work. Because the purpose is to compare the performance of the standard and newly derived decomposition methods of the modified surface vector, no algebraic multigrid solver is invoked during computations. Execution of the internal algebraic solver loop is continued until the residuals drop by two orders of magnitude.

### Test 1: Steady conduction with anisotropic coefficients

The first problem, schematically depicted in Figure 3(a) along with the imposed boundary conditions, deals with anisotropic conduction in a square domain of side 1. The enclosure is filled with orthotropic material of nonzero and zero conductivity in the  $\xi$ - and  $\eta$ -directions, respectively (i.e.,  $k_{\xi\xi} \neq 0$ ,  $k_{\eta\eta} = 0$ ). Thus, the solution is one-dimensional in the  $\xi$  direction, while it is two-dimensional in the  $(x, y)$  coordinate system and is given by [42, 54],

$$\phi = \begin{cases} x & y + x \tan(\gamma) - 1 < 0 \\ \left[ \frac{1-y}{1-y+(1-x)\tan(\gamma)} \right] * \left[ 1 + \frac{(1-x)\tan(\gamma)}{1-y} \left( x - \frac{1-y}{\tan(\gamma)} \right)^2 \right] & y + (x-1)\tan(\gamma) > 0 \\ x + \frac{y}{\tan(\gamma)} + y \left[ \left( x - \frac{1-y}{\tan(\gamma)} \right)^2 - \left( x + \frac{y}{\tan(\gamma)} \right) \right] & \text{else where} \end{cases} \quad (19)$$

where  $\gamma = \pi/2 - \theta$ .

The expressions for the diffusion tensors in the  $(\eta, \xi)$  and  $(x, y)$  coordinate systems are written as:

$$\mathbf{K}_{(\eta,\xi)} = \begin{pmatrix} k_{\eta\eta} & 0 \\ 0 & k_{\xi\xi} \end{pmatrix} \quad \mathbf{K}_{(x,y)} = \begin{pmatrix} k_{xx} & k_{xy} \\ k_{yx} & k_{yy} \end{pmatrix} \quad (20)$$

with the transformation relation allowing the calculation of  $\mathbf{K}_{(x,y)}$  from  $\mathbf{K}_{(\eta,\xi)}$  given by:

$$\mathbf{K}_{(x,y)} = \mathbf{R}^T(\theta) \mathbf{K}_{(\eta,\xi)} \mathbf{R}(\theta) \quad (21)$$

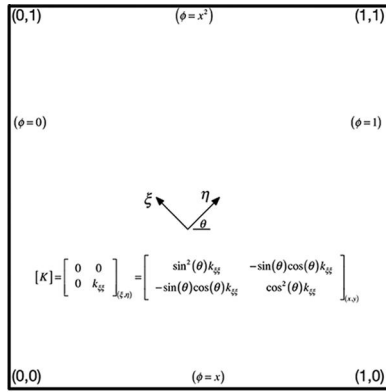
where  $\mathbf{R}(\theta)$  represents the rotation matrix for a transformation from the  $(x, y)$  to the  $(\eta, \xi)$  coordinate system and is expressed as:

$$\mathbf{R}(\theta) = \begin{bmatrix} \mathbf{e}_\eta \cdot \mathbf{i} & \mathbf{e}_\eta \cdot \mathbf{j} \\ \mathbf{e}_\xi \cdot \mathbf{i} & \mathbf{e}_\xi \cdot \mathbf{j} \end{bmatrix} \quad (22)$$

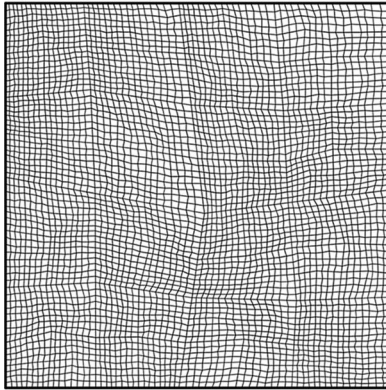
In Eq. (22),  $\mathbf{e}_\eta$  and  $\mathbf{e}_\xi$  are the unit vectors in the  $\eta$  and  $\xi$  directions, respectively, while  $\mathbf{i}$  and  $\mathbf{j}$  are the unit vectors in the  $x$  and  $y$  directions, respectively. Combining equations (20)–(22), and setting  $k_{\eta\eta} = 0$ ,  $k_{\xi\xi} = 1$ , and  $\theta = \pi/6$  (the values for which computations are performed), the diffusion tensor in the  $(x, y)$  coordinate system is obtained as:

$$\begin{pmatrix} k_{xx} & k_{xy} \\ k_{yx} & k_{yy} \end{pmatrix} = \begin{pmatrix} 1/4 & -\sqrt{3}/4 \\ -\sqrt{3}/4 & 3/4 \end{pmatrix} \quad (23)$$

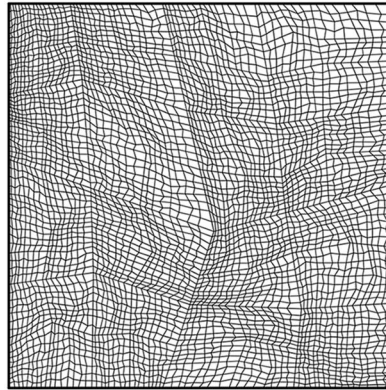
The domain is discretized using Shestakov-type grid systems [55] of different levels of skewness with its skewness coefficient  $\alpha$  varying between 0.5 and 0.3 with the value 0.5 resulting in an orthogonal Cartesian grid. For each skewness level, meshes with sizes of  $2^6$ ,  $2^8$ ,  $2^{10}$ ,  $2^{12}$ ,  $2^{14}$ ,  $2^{16}$ , and  $2^{18}$



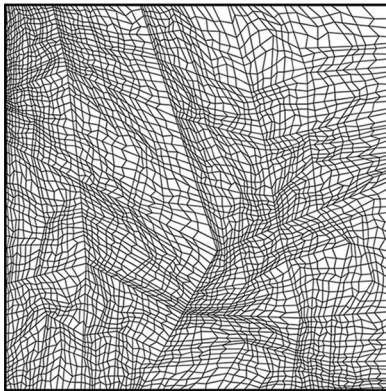
(a)



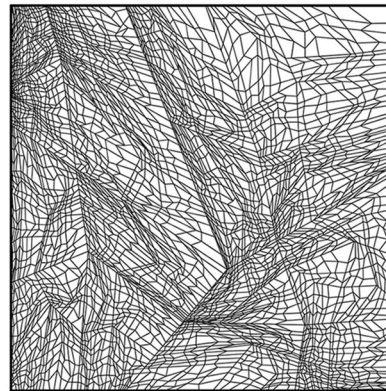
(b)



(c)



(d)



(e)

**Figure 3.** (a) Physical situation and boundary conditions for anisotropic diffusion in a square domain with an orthotropic material; Shestakov-type grid systems using  $2^{12}$  elements with (b)  $\alpha = 0.45$ , (c)  $\alpha = 0.4$ , (d)  $\alpha = 0.35$ , and (e)  $\alpha = 0.3$ .

quadrilateral elements are considered. Examples of the mesh systems used are displayed in Figures 3(b)–3(e) for a grid with size of  $2^{12}$  elements and for values of  $\alpha$  equal to 0.45 (Figure 3(b)), 0.4 (Figure 3(c)), 0.35 (Figure 3(d)), and 0.3 (Figure 3(e)). Further, the correctness of numerical results can be inferred from the comparison of  $\phi$ -contours generated analytically and numerically displayed in Figures 4(a) and 4(b), respectively.

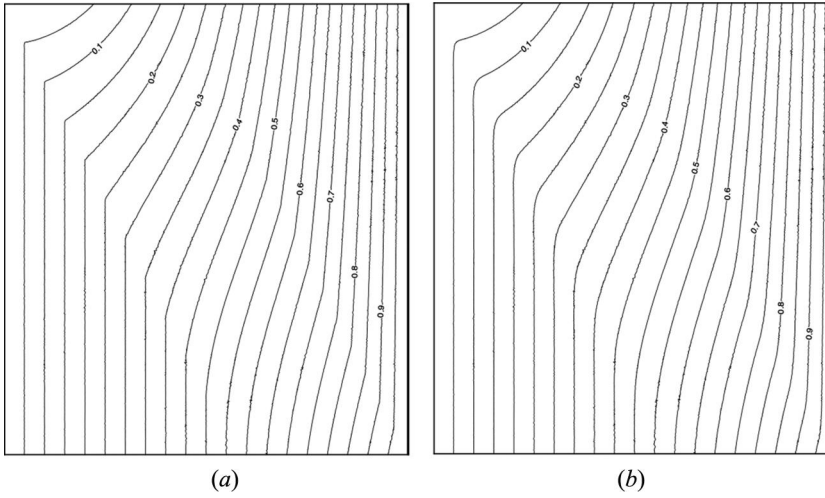


**Figure 4.**  $\phi$ -Contours for the anisotropic diffusion in a square domain problem obtained (a) from the exact solution and (b) numerically on a Shestakov-type grid ( $\alpha = 0.4$ ) with size of  $2^{18}$  elements.

The maximum and RMS numerical solution errors for all cases considered are displayed in Figure 5. These are defined as:

$$\begin{aligned} \text{Error}_{\max} &= \max_{i=1}^N |\phi_{i,\text{exact}} - \phi_{i,\text{numerical}}| \\ \text{Error}_{\text{RMS}} &= \sqrt{\frac{\sum_{i=1}^N (\phi_{i,\text{exact}} - \phi_{i,\text{numerical}})^2}{N}} \end{aligned} \quad (24)$$

where  $N$  is the total number of elements used. Plots in Figures 5(a)–5(e) are for grid systems with a skewness factor  $\alpha$  with value of 0.5, 0.45, 0.4, 0.35, and 0.3, respectively. For a given grid skewness, generated results clearly show the reduction in both maximum and RMS errors as the grid size increases. Further, for a given grid size, solution error increases as the grid skewness increases (compare plots in Figures 5(a)–5(e)). In all cases, the lowest solution error is obtained with the newly suggested method, i.e., when the modified surface vector is decomposed into its contravariant components. In addition, using the contravariant decomposition approach, errors obtained with both the SI and MIND schemes are almost identical. For grid systems with moderate skewness, i.e., for  $\alpha \geq 0.4$ , it was possible to obtain converged solutions with both decomposition approaches and with the SI and MIND schemes. Numerical difficulties with the standard decomposition start to appear for values of  $\alpha \leq 0.35$ . For  $\alpha = 0.35$ , it was not possible to get a converged solution with the SI scheme when the modified surface vector is decomposed following the standard approach. As  $\alpha$  is further decreased to 0.3, the only method that converges is the MIND scheme when the modified surface vector is decomposed in the contravariant directions. This clearly demonstrates the higher numerical robustness of both the MIND scheme and the contravariant modified surface vector decomposition approach.

The CPU times required by the various methods for the maximum absolute residual over the domain to drop below  $10^{-8}$  are presented in Figures 6(a)–6(e) for meshes with a skewness factor  $\alpha$  of value 0.5, 0.45, 0.4, 0.35, and 0.3, respectively. In each figure, the variations of CPU time with grid size are presented for the MIND and SI schemes with the modified surface vector decomposed following the standard and contravariant approach. As expected, the computational time increases with the grid size and for a given grid size it increases as the skewness of the grid increases. The computational time required by the MIND scheme is higher than the one needed by the SI scheme to

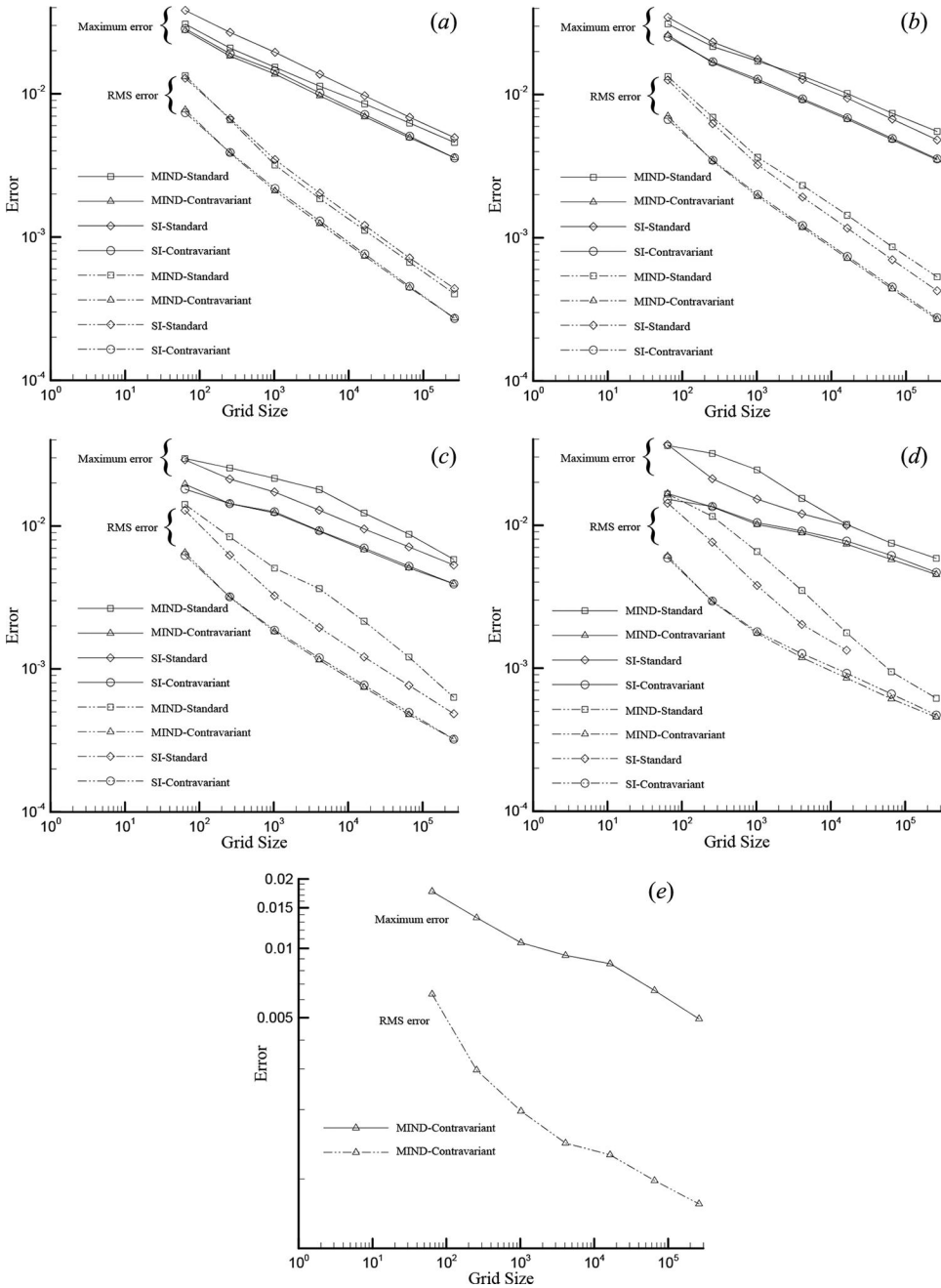


**Figure 5.** Variation of maximum and RMS errors with grid size for the anisotropic diffusion in a square domain problem using the SI and MIND schemes with the two modified surface decomposition methods for Shestakov-type grids with (a)  $\alpha = 0.5$ , (b)  $\alpha = 0.45$ , (c)  $\alpha = 0.4$ , (d)  $\alpha = 0.35$ , and (e)  $\alpha = 0.3$ . Note: MIND, modified implicit nonlinear diffusion.

reach the required level of convergence. However, the MIND scheme is numerically more robust and is the only one capable of producing a converged solution at the highest skewness considered, i.e., for  $\alpha = 0.3$ . Most importantly however, is the fact that for both discretization methods, the contravariant decomposition practice requires much lower computational time than the standard decomposition approach with the differences increasing as the grid size increases. As can be seen, the contravariant

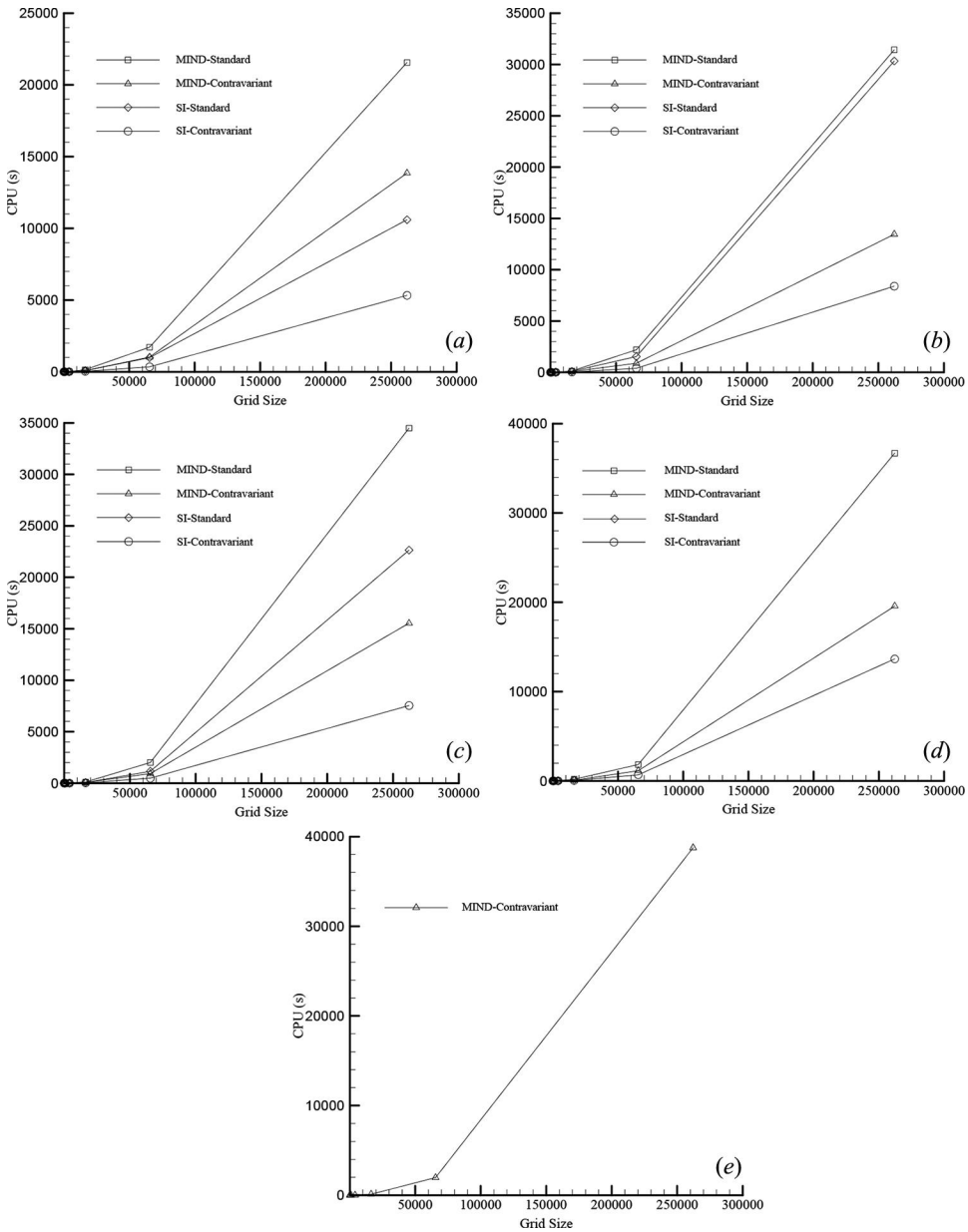


**Figure 6.** Variation of CPU time with grid size for the anisotropic diffusion in a square domain problem using the SI and MIND schemes with the two modified surface decomposition methods for Shestakov-type grids with (a)  $\alpha = 0.5$ , (b)  $\alpha = 0.45$ , (c)  $\alpha = 0.4$ , (d)  $\alpha = 0.35$ , and (e)  $\alpha = 0.3$ . Note: MIND, modified implicit nonlinear diffusion.

decomposition approach requires a fraction of the time required by the standard decomposition technique for both the MIND and SI schemes. The reduction in CPU time varies with the grid size and grid skewness and reaches a value as high as 70%. The MIND scheme with the contravariant decomposition of the modified surface vector is the only combination that converges for all grid systems used.

Figure 7 further compares the performance of the various schemes by plotting, over the densest grid used, the reduction in residuals with iterations for different values of the skewness factor, i.e., for  $\alpha = 0.5$  (Figure 7(a)),  $\alpha = 0.45$  (Figure 7(b)),  $\alpha = 0.4$  (Figure 7(c)),  $\alpha = 0.35$  (Figure 7(d)),

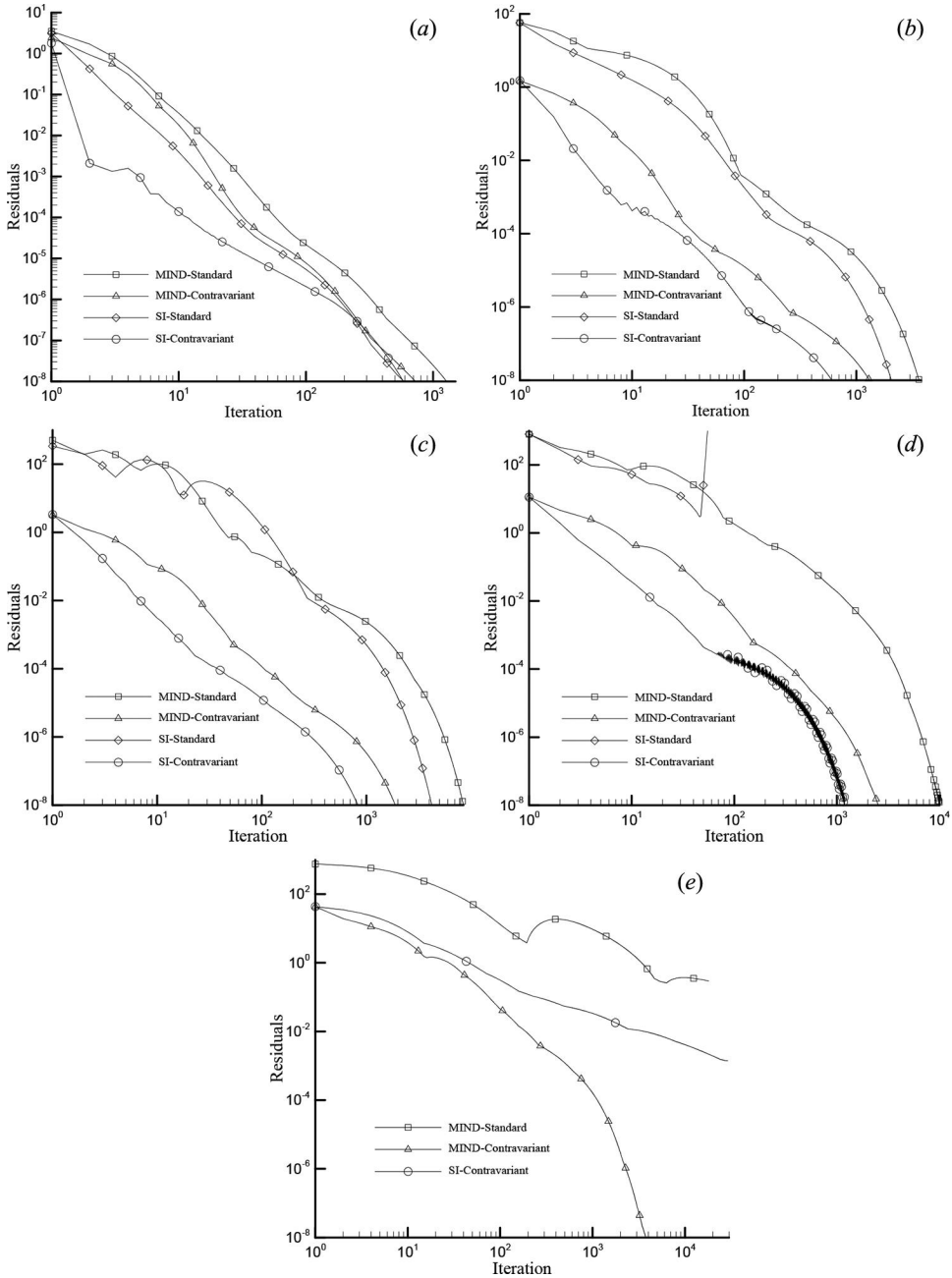


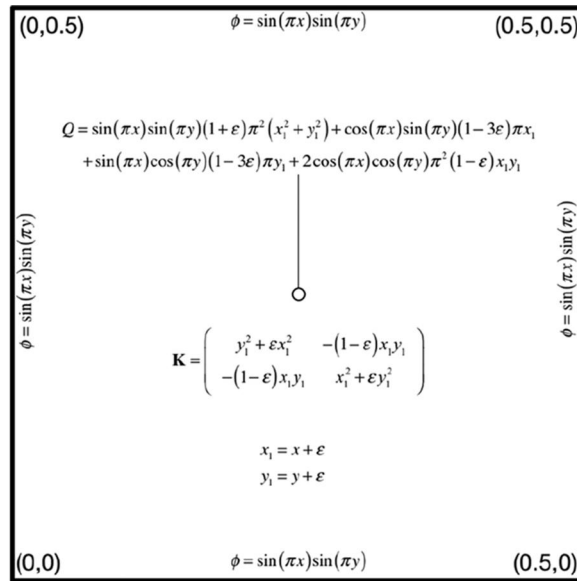
**Figure 7.** Reduction of residuals with iterations for the anisotropic diffusion in a square domain problem using the SI and MIND schemes with the two modified surface decomposition methods for Shestakov-type grid systems with size of  $2^{18}$  quadrilateral elements with (a)  $\alpha = 0.5$ , (b)  $\alpha = 0.45$ , (c)  $\alpha = 0.4$ , (d)  $\alpha = 0.35$ , and (e)  $\alpha = 0.3$ . Note: MIND, modified implicit nonlinear diffusion.

and  $\alpha = 0.3$  (Figure 7(e)). As shown, the lowest number of iterations is always associated with the contravariant decomposition approach of the modified surface vector. The divergence of computations when solving the problem using the SI scheme with the standard decomposition approach for a skewness factor  $\alpha = 0.35$  is clearly shown in Figure 7(d). Further, for  $\alpha = 0.3$  (Figure 7(e)), the only method that produces a converged solution is the MIND scheme with a contravariant

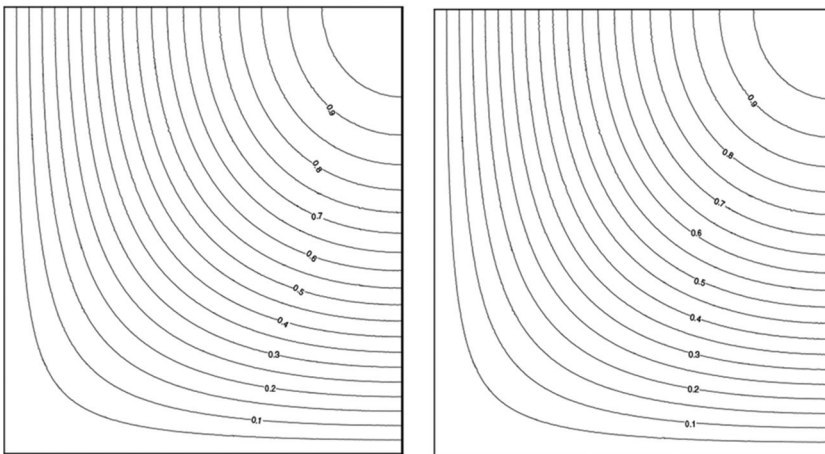
decomposition of the modified surface vector. Further, the convergence rates of the SI and MIND schemes using a contravariant and a standard decomposition of  $\mathbf{S}'$ , respectively, are very slow. The computations for these two cases were not completed because after a large number of iterations their residuals are still at least five orders of magnitude higher than the level set for convergence. In addition, for the same case, the SI scheme with a standard decomposition of  $\mathbf{S}'$ , diverged after few iterations and is not presented in the figure.

**Test 2: Anisotropic conduction with a distributed source term**

Figure 8(a) displays a schematic of the problem along with its boundary conditions [40, 44, 46]. The domain consists of a square of side 0.5 over which the distribution of a property  $\phi$  in the presence of



(a)



(b)

(c)

**Figure 8.** (a) Physical situation and boundary conditions for anisotropic diffusion in a square domain with a distributed source term;  $\phi$ -contours, (b) obtained from the exact solution, and (c) generated numerically on a Shestakov-type grid ( $\alpha = 0.4$ ) with size of  $2^{18}$  elements.

a source term  $Q$  is sought. The domain is filled with anisotropic material of diffusion coefficient tensor  $\mathbf{K}$ . The expressions for both  $\mathbf{K}$  and  $Q$  are given in Figure 8(a). The value of  $\phi$  at all boundaries is set to

$$\phi = \sin(\pi x) \sin(\pi y) \tag{25}$$

The analytical solution for the problem is also given by Eq. (25). Moreover, grid systems similar to the ones used in solving the previous problem are used here, i.e., Shestakov-type grids [55] with sizes of  $2^6, 2^8, 2^{10}, 2^{12}, 2^{14}, 2^{16}$ , and  $2^{18}$  quadrilateral elements and for each grid size five mesh systems of

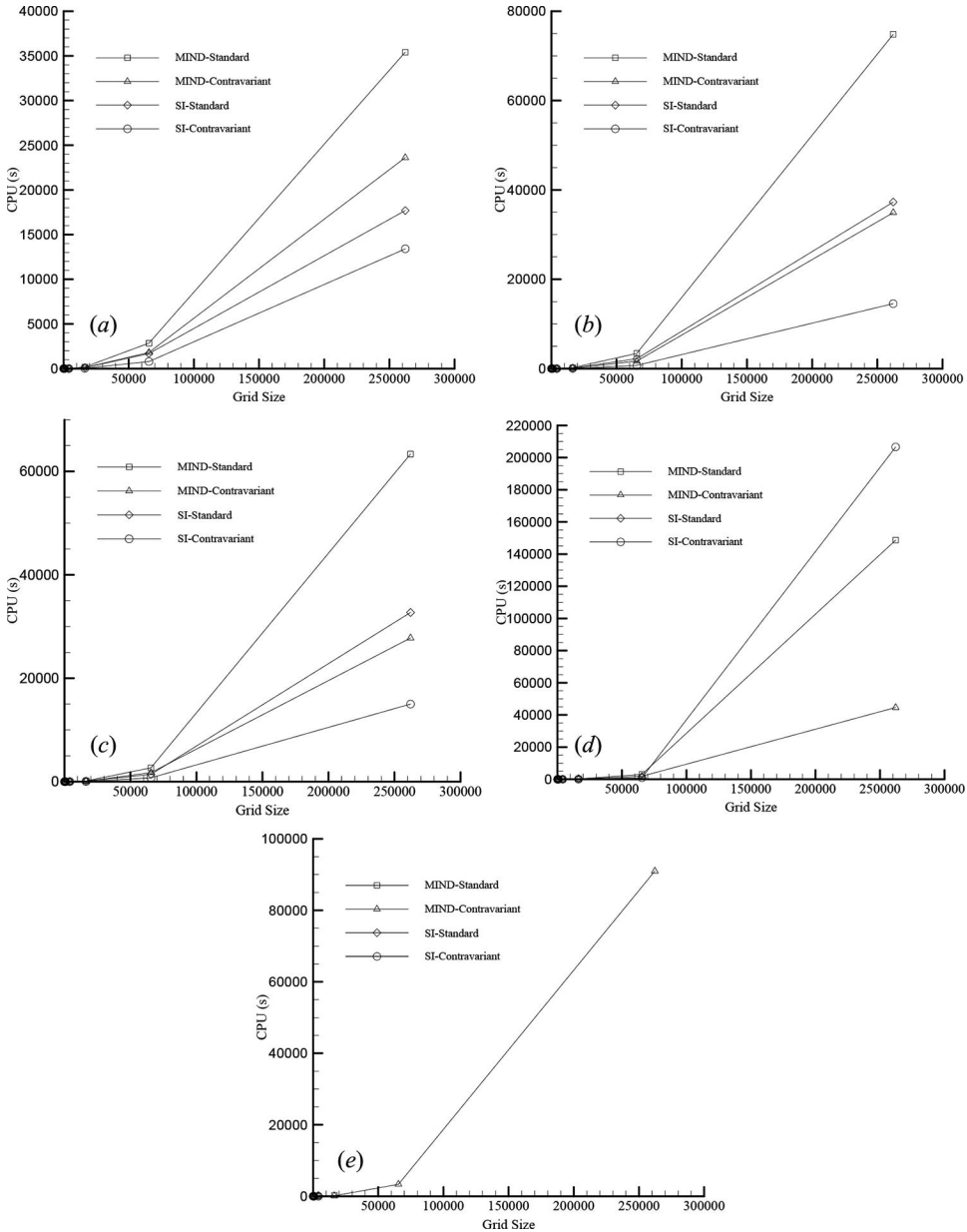


**Figure 9.** Variation of CPU time with grid size for anisotropic diffusion in a square domain with a distributed source term using the SI and MIND schemes with the two modified surface decomposition methods for Shestakov-type grids with (a)  $\alpha = 0.5$ , (b)  $\alpha = 0.45$ , (c)  $\alpha = 0.4$ , (d)  $\alpha = 0.35$ , and (e)  $\alpha = 0.3$ . Note: MIND, modified implicit nonlinear diffusion.

different skewnesses ( $0.3 \leq \alpha \leq 0.5$ ). Solutions are generated with  $\epsilon$  set to  $10^{-7}$  resulting in an anisotropic ratio of value  $10^7$ . The accuracy of results can be inferred from the analytical and numerical solutions presented in the form of  $\phi$ -contours in Figures 8(b) and 8(c), respectively.

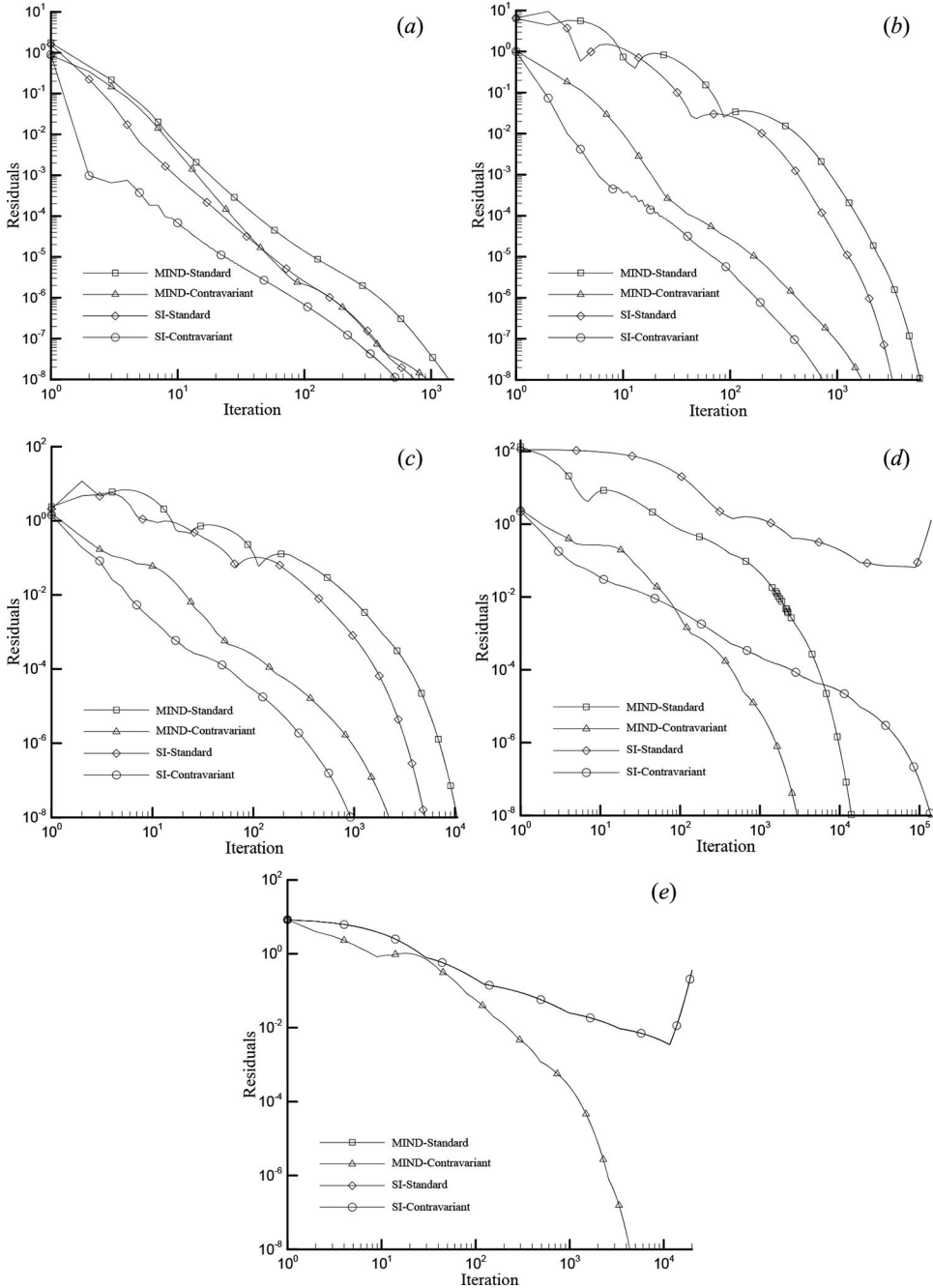


**Figure 10.** Reduction of residuals with iterations for anisotropic diffusion in a square domain with a distributed source term using the SI and MIND schemes with the two modified surface decomposition methods for Shestakov-type grid systems with size of  $2^{18}$  quadrilateral elements with (a)  $\alpha = 0.5$ , (b)  $\alpha = 0.45$ , (c)  $\alpha = 0.4$ , (d)  $\alpha = 0.35$ , and (e)  $\alpha = 0.3$ . Note: MIND, modified implicit nonlinear diffusion.

The computational times required for convergence, i.e., for the residuals to be decreased to the set level, for all cases considered are depicted in Figure 9. As in Figure 6, the CPU times, for a given grid skewness, are plotted as a function of the grid size for the different discretization and modified surface vector decomposition methods. Results are reported in Figures 9(a)–(e) for meshes with a skewness factor  $\alpha$  of value 0.5, 0.45, 0.4, 0.35, and 0.3, respectively. The same trend of results obtained in the previous problem is repeated here. The CPU time increases with increasing the grid size and/or the grid skewness. Using the modified surface vector decomposition method, the SI scheme requires lower computational time than the MIND scheme for low and moderate grid skewness. However, for highly skewed grid, the MIND scheme is more robust and more efficient than the SI scheme. As shown in Figure 9(d), the CPU time required by the MIND scheme is almost one-fifth the CPU time needed by the SI method. In addition, on the grid system with the highest skewness (i.e.,  $\alpha = 0.3$ ), Figure 9(e) indicates that the MIND scheme with the contravariant decomposition approach is the only combination that converges to a solution for all grid sizes. Again the newly suggested contravariant decomposition approach consistently requires a fraction of the time required by the standard decomposition technique for both the MIND and SI schemes.

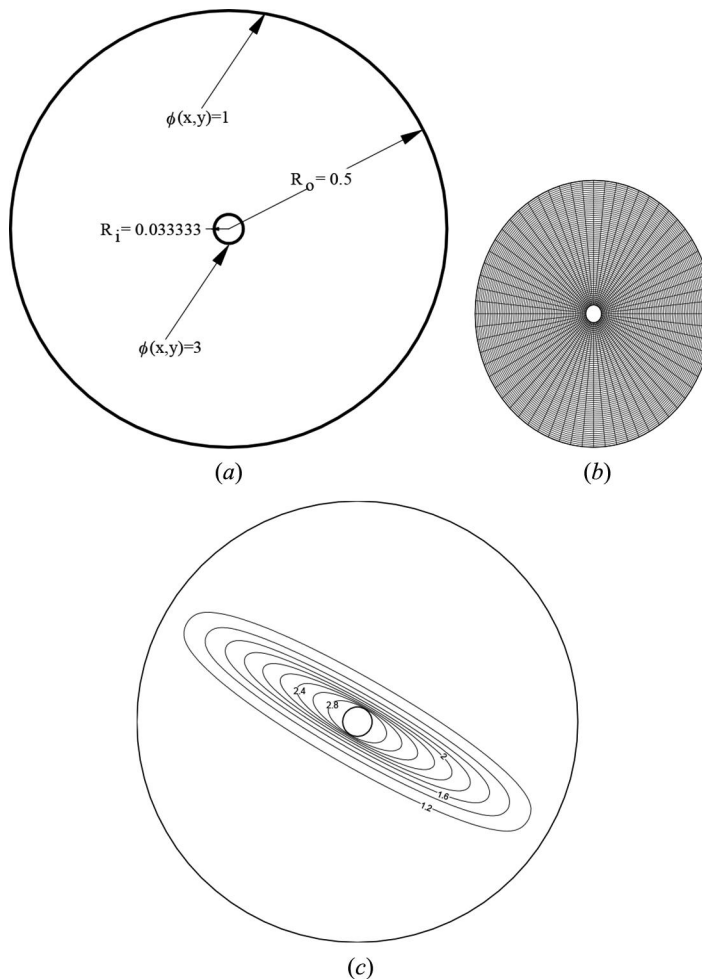


**Figure 11.** (a) Physical situation and boundary conditions for the anisotropic conduction in a hollow cylinder problem; (b) an illustrative grid network with quadrilateral elements used; (c)  $\phi$ -contours generated numerically over a grid systems with size of  $2^{18}$  quadrilateral elements.

The above findings are further confirmed by the residual history plots presented in Figures 10(a)–10(e). For a given grid skewness, results on the densest grid are reported for the various discretization methods used. For low grid skewness (Figures 10(a)–(c)), the SI scheme requires lower number of iterations for convergence with the lowest number always obtained when decomposing the modified surface vector using the contravariant approach. For higher grid skewness (Figure 10(d)), the SI scheme with the standard decomposition of the modified surface vector does not converge, while heavy underrelaxation is required to promote convergence of the SI scheme with the contravariant decomposition approach leading to a large increase in the required number of iterations and consequently the CPU time. The best performance in this case is obtained with the MIND scheme when decomposing  $\mathbf{S}'$  in the contravariant directions. Again for the grid with the highest skewness ( $\alpha = 0.3$ , Figure 10(e)), the only scheme that converges is the MIND scheme with  $\mathbf{S}'$  decomposed using the contravariant approach. The other schemes diverge either directly (do not appear in the figure due to the low number of iterations from the start of computations to divergence) or after many iterations. In all cases, the least number of iterations is obtained when the modified surface vector is decomposed using the contravariant approach.

### Test 3: Anisotropic conduction in a hollow cylinder

The last problem, schematically displayed in Figure 11(a), deals with anisotropic conduction in a hollow cylinder of outer and inner diameters 1 and 1/15, respectively. The anisotropic conductivity tensor is obtained by rotation of the diagonal diffusion tensor given by:

$$\mathbf{K}_{(\eta, \xi)} = \begin{pmatrix} 1 & 0 \\ 0 & \varepsilon \end{pmatrix} \quad (26)$$

through an angle  $\theta = \pi/3$ . Setting the value of  $\varepsilon$  to 100, the anisotropic diffusion tensor in the  $(x, y)$  coordinate system is obtained from Eq. (21) as:

$$\mathbf{K}_{(x,y)} = \begin{pmatrix} \frac{301}{4} & \frac{-99\sqrt{3}}{4} \\ \frac{-99\sqrt{3}}{4} & \frac{103}{4} \end{pmatrix} \quad (27)$$

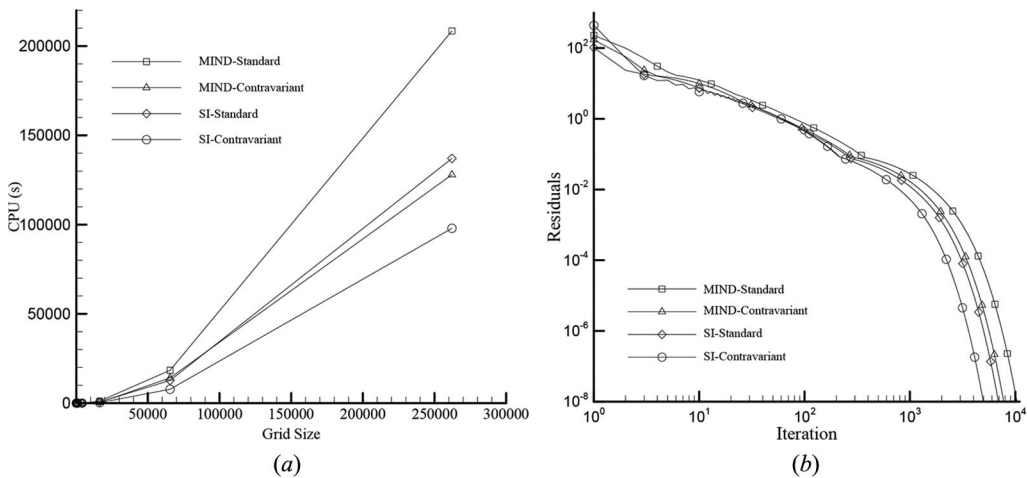


**Figure 12.** (a) Variation of CPU time with grid size and (b) reduction of residuals over a grid system with size of  $2^{18}$  quadrilateral elements with iteration for the anisotropic conduction in a hollow cylinder problem using the SI and MIND schemes with the two modified surface decomposition methods. *Note:* MIND, modified implicit nonlinear diffusion.

The problem is solved over seven O-type grid systems with sizes of  $2^6$ ,  $2^8$ ,  $2^{10}$ ,  $2^{12}$ ,  $2^{14}$ ,  $2^{16}$ , and  $2^{18}$  quadrilateral elements subject to a Dirichlet condition of  $\phi = 1$  on the outer boundaries and  $\phi = 3$  on the inner boundaries. Figure 11(b) depicts an illustrative grid network used, while Figure 11(c) displays the  $\phi$ -contours numerically generated over the domain. The problem is solved using the various discretization techniques and a summary of the computational time required for all cases considered along with illustrative residual history plots is presented in Figure 12. Again, results reported in Figure 12(a) indicate that the SI scheme is more efficient for smooth grid systems, while the contravariant decomposition approach requires the lowest computational time for a converged solution to be obtained. This is further revealed in Figure 12(b), which displays the residual history plots for the densest grid used. Again the lowest number of iterations results when the modified surface vector is decomposed following the contravariant approach.

## Closing remarks

The paper dealt with a new decomposition approach for the discretization of the anisotropic diffusion operator. The method is based on decomposing the modified surface vector into two components that are aligned with the grid system (i.e., the contravariant components). The new method was compared to the standard practice in which the modified surface vector ( $S'$ ) is split into two components; one aligned with the grid, while the other component was orthogonal to  $S'$ . The new and standard decomposition practices were embedded in a computer code in which the SI and MIND diffusion schemes are implemented and used to solve several anisotropic diffusion problems. Results generated indicated that the SI scheme is more efficient than the MIND scheme on grid systems of moderate skewness. The MIND scheme is more robust than the SI scheme and is more efficient on highly skewed grid systems. For the grid system with the highest skewness considered in this study, the SI scheme failed to converge. Moreover, for all cases considered, decomposing the modified surface vector in the contravariant directions resulted in a sizable reduction of CPU time reaching a value as high as 70%.

## Funding

This work was supported by the American University of Beirut [Grant Number 103371].

## References

- [1] S. V. Patankar, "A calculation procedure for two dimensional elliptic situations," *Numer. Heat Transfer*, vol. 4, no. 4, pp. 409–425, 1981. DOI:10.1080/10407798108547025
- [2] S. V. Patankar, *Numerical Heat Transfer and Fluid Flow*. New York, NY: Hemisphere Publishing, 1980.
- [3] S. V. Patankar and D. B. Spalding, "A calculation procedure for heat, mass and momentum transfer in three-dimensional parabolic flows," *Int. J. Heat Mass Transfer*, vol. 15, no. 10, pp. 1787–1806, 1972. DOI:10.1016/b978-0-08-030937-8.50013-1
- [4] F. Moukalled, L. Mangani, and M. Darwish. *The Finite Volume Method in Computational Fluid Dynamics: An Advanced Introduction with OpenFOAM® and Matlab®*. Springer, Switzerland, 2015.
- [5] G. D. Raithby and G. E. Schneider, "Numerical solution of problems in incompressible fluid flow: treatment of the velocity-pressure coupling," *Numer. Heat Transfer*, vol. 2, no. 4, pp. 417–440, 1979. DOI:10.1080/10407797908547089
- [6] S. V. Patankar, "Numerical prediction of three-dimensional flow," In *Studies in Convection: Theory, Measurement, and Application*, vol. 1, B. E. Launder Ed. New York: Academic, 1975, pp. 1–9.
- [7] C. M. Rhie and W. L. Chow, "Numerical study of the turbulent flow past an airfoil with trailing edge separation," *AIAA J.*, vol. 21, pp. 1525–1532, 1983. DOI:10.2514/3.8284
- [8] B. P. Leonard, "A stable and accurate convective modelling procedure based on quadratic upstream interpolation," *Comput. Methods Appl. Mech. Eng.*, vol. 19, pp. 59–98, 1979. DOI:10.1016/0045-7825(79)90034-3
- [9] P. H. Gaskell and A. K. C. Lau, "Curvature compensated convective transport: SMART, a new boundedness preserving transport algorithm," *Int. J. Numer. Methods Fluids*, vol. 8, no. 6, pp. 617–641, 1988. DOI:10.1002/flid.1650080602

- [10] E. A. Fromm, "A method for reducing dispersion in convective difference schemes," *J. Comput. Phys.*, vol. 3, pp. 176–189, 1968. DOI:[10.1016/0021-9991\(68\)90015-6](https://doi.org/10.1016/0021-9991(68)90015-6)
- [11] B. P. Leonard and H. S. Nikkaffs, "Sharp monotonic resolution of discontinuities without clipping of narrow extrema," *Comput. Fluids*, vol. 19, pp. 141–154, 1991. DOI:[10.1016/0045-7930\(91\)90011-6](https://doi.org/10.1016/0045-7930(91)90011-6)
- [12] B. Van Leer, "Towards the ultimate conservation difference scheme V. A second order sequel to Godunov's method," *J. Comput. Phys.*, vol. 23, pp. 101–136, 1977. DOI:[10.1016/0021-9991\(79\)90145-1](https://doi.org/10.1016/0021-9991(79)90145-1)
- [13] J. Zhu and W. Rodi, "A low-dispersion and bounded convection scheme," *Comput. Methods Appl. Mechan. Eng.*, vol. 92, pp. 87–96, 1991. DOI:[10.1016/0045-7825\(91\)90199-g](https://doi.org/10.1016/0045-7825(91)90199-g)
- [14] H. C. Yee, R. F. Warming, and A. Harten, Implicit total variation diminishing (TVD) schemes for steady-state calculations, NASA Technical Memorandum 84832, 1983.
- [15] P. K. Sweby, "High resolution schemes using flux limiters for hyperbolic conservation Laws," *SIAM J. Numer. Anal.*, vol. 21, no. 5, pp. 995–1011, 1984. DOI:[10.1137/0721062](https://doi.org/10.1137/0721062)
- [16] B. P. Leonard, "Simple high-accuracy resolution program for convective modelling of discontinuities," *Int. J. Numer. Methods Eng.*, vol. 8, pp. 1291–1318, 1988. DOI:[10.1002/flid.1650081013](https://doi.org/10.1002/flid.1650081013)
- [17] M. Darwish, "A new high resolution scheme based on the normalized variable formulation," *Numer. Heat Transfer, Part B*, vol. 24, pp. 353–371, 1993. DOI:[10.1080/10407799308955898](https://doi.org/10.1080/10407799308955898)
- [18] M. Darwish and F. Moukalled, "Normalized variable and space formulation methodology for high-resolution schemes," *Numer. Heat Transfer, Part B*, vol. 26, no. 1, pp. 79–96, 1994. DOI:[10.1080/10407799408914918](https://doi.org/10.1080/10407799408914918)
- [19] F. Moukalled and M. Darwish, "New family of adaptive very high resolution schemes," *Numer. Heat Transfer, Part B*, vol. 34, pp. 215–239, 1998. DOI:[10.1080/10407799808915055](https://doi.org/10.1080/10407799808915055)
- [20] M. Darwish and F. Moukalled, "The schemes: a new consistent high-resolution formulation based on the normalized variable methodology," *Comput. Methods Appl. Mechan. Eng.*, vol. 192, pp. 1711–1730, 2003. DOI:[10.1016/s0045-7825\(03\)00199-3](https://doi.org/10.1016/s0045-7825(03)00199-3)
- [21] M. Darwish and F. Moukalled, "TVD schemes for unstructured grids," *Int. J. Heat Mass Transfer*, vol. 46, no. 4, pp. 599–611, 2003. DOI:[10.1016/s0017-9310\(02\)00330-7](https://doi.org/10.1016/s0017-9310(02)00330-7)
- [22] L. Mangani, L. Buchmayr, and M. Darwish, "Development of a novel fully coupled solver in openfoam: steady-state incompressible turbulent flows," *Numer. Heat Transfer, Part B*, vol. 66, no. 1, pp. 1–20, 2014. DOI:[10.1080/10407790.2014.894448](https://doi.org/10.1080/10407790.2014.894448)
- [23] S.-K. Choi, S.-O. Kim, T.-H., Lee, and D. H. Dohee, "Computation of the natural convection of nanofluid in a square cavity with homogeneous and nonhomogeneous models," *Numer. Heat Transfer, Part A*, vol. 65, no. 4, pp. 287–301, 2014. DOI:[10.1080/10407782.2013.831695](https://doi.org/10.1080/10407782.2013.831695)
- [24] S.-J. Liang, Y.-J. Jan, and C.-A. Huang, "A quasi-implicit time-advancing scheme for flow in a three-dimensional curved duct," *Numer. Heat Transfer, Part B*, vol. 64, no. 4, pp. 306–325, 2013. DOI:[10.1080/10407790.2013.806203](https://doi.org/10.1080/10407790.2013.806203)
- [25] S. Vakili-pour and S. J. Ormiston, "A coupled pressure-based co-located finite-volume solution method for natural-convection flows," *Numer. Heat Transfer, Part B*, vol. 61, no. 2, pp. 91–115, 2012. DOI:[10.1080/10407790.2012.642281](https://doi.org/10.1080/10407790.2012.642281)
- [26] S. Das, S. R. Mathur, and J. Y. Murthy, "Finite-volume method for creep analysis of thin RF MEMS devices using the theory of plates," *Numer. Heat Transfer, Part B*, vol. 61, no. 2, pp. 71–90, 2012. DOI:[10.1080/10407790.2012.646170](https://doi.org/10.1080/10407790.2012.646170)
- [27] S. Das, S. R. Mathur, and J. Y. Murthy, "Finite-volume method for structural analysis of RF MEMS devices using the theory of plates," *Numer. Heat Transfer, Part B*, vol. 61, no. 1, pp. 1–21, 2012. DOI:[10.1080/10407790.2011.630949](https://doi.org/10.1080/10407790.2011.630949)
- [28] S.-K. Choi and C.-L. Lin, "A simple finite-volume formulation of the lattice Boltzmann method for laminar and turbulent flows," *Numer. Heat Transfer, Part B*, vol. 58, no. 4, pp. 242–261, 2010. DOI:[10.1080/10407790.2010.511965](https://doi.org/10.1080/10407790.2010.511965)
- [29] H. M. Matos, M. A. Alves, and P. J. Oliveira, "New formulation for stress calculation: Application to viscoelastic flow in a T-junction," *Numer. Heat Transfer, Part B*, vol. 56, no. 5, pp. 351–371, 2009. DOI:[10.1080/10407790903507972](https://doi.org/10.1080/10407790903507972)
- [30] A. Dalal, V. Eswaran, and G. Biswas, "A finite-volume method for Navier-stokes equations on unstructured meshes," *Numer. Heat Transfer, Part B*, vol. 54, no. 3, pp. 238–259, 2008. DOI:[10.1080/10407790802182653](https://doi.org/10.1080/10407790802182653)
- [31] V. C. Mariani and A. T. Prata, "A Eulerian-Lagrangian method applied to fluid flow in lid-driven cavities with irregular bottom walls," *Numer. Heat Transfer, Part B*, vol. 53, no. 3, pp. 206–233, 2008. DOI:[10.1080/10407790701632568](https://doi.org/10.1080/10407790701632568)
- [32] C. D. Perez-Segarra, C. Farre, J. Cadafalch, and A. Oliva, "Analysis of different numerical schemes for the resolution of convection-diffusion equations using finite-volume methods on three-dimensional unstructured grids. Part I: discretization schemes," *Numer. Heat Transfer, Part B*, vol. 49, no. 4, pp. 333–350, 2006. DOI:[10.1080/10407790500314947](https://doi.org/10.1080/10407790500314947)
- [33] W. J. Ferguson and I. W. Turner, "Study of two-dimensional cell-centered and vertex-centered control-volume schemes applied to high-temperature timber drying," *Numer. Heat Transfer, Part B*, vol. 27, no. 4, pp. 393–415, 1995. DOI:[10.1080/10407799508914964](https://doi.org/10.1080/10407799508914964)

- [34] I. Demirdzic, “A finite volume method for computation of fluid flow in complex geometries,” Ph.D. thesis, University of London, London, UK, 1982.
- [35] S. Muzaferija, “Adaptive finite volume method for flow predictions using unstructured meshes and multigrid approach,” Ph.D. thesis, University of London, London, UK, 1994.
- [36] I. Demirdzic and S. Muzaferija, “Numerical method for coupled fluid flow, heat transfer and stress analysis using unstructured moving meshes with cells of arbitrary topology,” *Comput. Methods Appl. Mech. Eng.*, vol. 125, pp. 235–255, 1995.
- [37] S. R. Mathur and J. Y. Murthy, “A pressure-based method for unstructured meshes,” *Numer. Heat Transfer, Part B*, vol. 31, pp. 195–215, 1997. DOI:10.1080/10407799708915105
- [38] H. Jasak, “Error analysis and estimation for the finite volume method with applications to fluid flow,” Ph.D. thesis, Imperial College, London, 1996.
- [39] I. Demirdzic, “On the discretization of the diffusion term in finite-volume continuum mechanics,” *Numer. Heat Transfer, Part B*, vol. 68, no. 1, pp. 1–10, 2015.
- [40] M. Darwish and F. Moukalled, “A compact procedure for discretization of the anisotropic diffusion operator,” *Numer. Heat Transfer, Part B*, vol. 55, no. 5, pp. 339–360, 2009. DOI:10.1080/10407790902816747
- [41] S. G. Rubin and P. K. Khosla, “Polynomial interpolation method for viscous flow calculations,” *J. Comput. Phys.*, vol. 27, pp. 153–168, 1982. DOI:10.1016/0021-9991(77)90036-5
- [42] I. Aavatsmark, “An introduction to multipoint flux approximations for quadrilateral grids,” *Comput. Geosci.*, vol. 6, pp. 405–432, 2002.
- [43] I. Aavatsmark, G. Eigestad, B. Mallison, and J. Nordbotten, “A compact multipoint flux approximation method with improved robustness,” *Numer. Methods Partial Differ. Equations*, vol. 24, no. 5, pp. 1329–1360, 2008. DOI:10.1002/num.20320
- [44] C. LePotier, “Schema volumes finis monotone pour des operateurs de diffusion fortement anisotropes sur des maillages de triangle non structures,” *Comptes Rendus Mathématiques*, vol. 341, pp. 787–792, 2005.
- [45] F. Brezzi, K. Lipnikov, M. Shashkov, and V. Simoncini, “A new discretization methodology for diffusion problems on generalized polyhedral meshes,” *Comput. Methods Appl. Mech. Eng.*, vol. 196, pp. 3682–3692, 2007. DOI:10.1016/j.cma.2006.10.028
- [46] K. Lipnikov, D. Svyatskiy, M. Shashkov, and Y. Vassilevski, “Monotone Finite volume schemes for diffusion equations on unstructured triangular and shape-regular polygonal meshes,” *J. Comput. Phys.*, vol. 227, pp. 492–512, 2007. DOI:10.1016/j.jcp.2007.08.008
- [47] K. Lipnikov, D. Svyatskiy, and Y. Vassilevski, “Interpolation-free monotone finite volume method for diffusion equations on polygonal meshes,” *J. Comput. Phys.*, vol. 228, pp. 703–716, 2009. DOI:10.1016/j.jcp.2008.09.031
- [48] K. Nikitin and Y. Vassilevski, “A monotone nonlinear finite volume method for advection–diffusion equations on unstructured polyhedral meshes in 3D,” *Russ. J. Numer. Anal. Math. Modell.*, vol. 25, no. 4, pp. 335–358, 2010. DOI:10.1515/rjnamm.2010.022
- [49] G. Manzini and M. Putti, “Mesh locking effects in the finite volume solution of 2-D anisotropic diffusion equations,” *J. Comput. Phys.*, vol. 220, pp. 751–771, 2007. DOI:10.1016/j.jcp.2006.05.026
- [50] I. Kapyrin, “A family of monotone methods for the numerical solution of three-dimensional diffusion problems on unstructured tetrahedral meshes,” *Doklady Math.*, vol. 76, no. 2, pp. 734–738, 2007. DOI:10.1134/S1064562407050249
- [51] M. Darwish, L. Mangani, and F. Moukalled, “General fully implicit discretization of the diffusion term for the finite volume method,” *Numer. Heat Transfer, Part B*, vol. 71, no. 6, pp. 506–532, 2017. DOI:10.1080/10407790.2017.1330060
- [52] K. Lipnikov, D. Svyatskiy, and Y. Vassilevski, “A monotone finite volume method for advection-diffusion equations on unstructured polygonal meshes,” *J. Comput. Phys.*, vol. 229, pp. 4017–4032, 2010. DOI:10.1016/j.jcp.2010.01.035
- [53] V. S. Borisov and S. Sorek, “On the monotonicity of difference schemes for computational physics,” *SIAM J. Sci. Comput.*, vol. 25, pp. 1557–1584, 2004.
- [54] M. Keyhani and R. A. Polehn, “Finite difference modeling of anisotropic flows,” *ASME J. Heat Transfer*, vol. 117, pp. 458–464, 1995. DOI:10.1115/1.2822544
- [55] A. I. Shestakov, D. S. Kershaw, and G. B. Zimmerman, “Test problems in radiative transfer calculations,” *Nucl. Sci. Eng.*, vol. 105, no. 1, pp. 88–104, 1990. DOI:10.13182/nse90-a19215